

Si_{1-x}Ge_x/Si heterojunction infrared photoemission long wavelength infrared detector

T. J. Jin, J. S. Park, S. D. Guongah, J. W. Jones, and H. M. Del Castillo

Center for Space Microelectronics Technology, Jet Propulsion Laboratory
California Institute of Technology, 4800 Oak Grove Dr., Pasadena, CA 91109

ABSTRACT

Long wavelength Si_{1-x}Ge_x/Si heterojunction infrared photoemission (HIP) infrared detectors have been successfully demonstrated utilizing the growth of degenerately boron doped Si_{1-x}Ge_x layers on Si. Recently, Si_{0.75}Ge_{0.25}/Si HIP detectors with either a Si_{1-x}Ge_x/Si single layer or a Si_{1-x}Ge_x/Si multi layer have been demonstrated with cutoff wavelengths out to 23 μm. Near-ideal thermionic emission dark current characteristics were measured and the electrical potential barriers were determined by the Richardson plot. A photoresponse model, similar to the modified Fowler Equation has been developed for the Si_{1-x}Ge_x/Si heterojunction infrared photoemission (HIP) infrared detector at wavelengths corresponding to photon energies less than the Fermi energy. The optical potential barriers, the corresponding cutoff wavelengths, and the emission coefficients, C₁, for the HIP detectors have been determined from the measured spectral responses using the photoresponse model. Similar optical and thermal potential barriers were obtained.

1. INTRODUCTION

Currently, the PrSi Schottky infrared (IR) detector offers focal plane arrays (FPAs) with the largest array dimension and the best uniformity due to the superior material properties of Si and the mature Si-based processing technologies¹. However, PrSi FPAs are limited to MWIR applications due to the 5.1-5.9 μm cutoff wavelength, given by $\lambda_c = 1.24/\eta^2$, where $\eta = 0.22$ eV is the Schottky barrier of PrSi on p-type Si. In 1971, Shepherd et al. proposed a semiconductor IR detector which replace the schiade electrode of the Schottky IR detector with a degenerately-doped semiconductor². The proposed detector promised an improved emission coefficient due to the reduced Fermi energy.

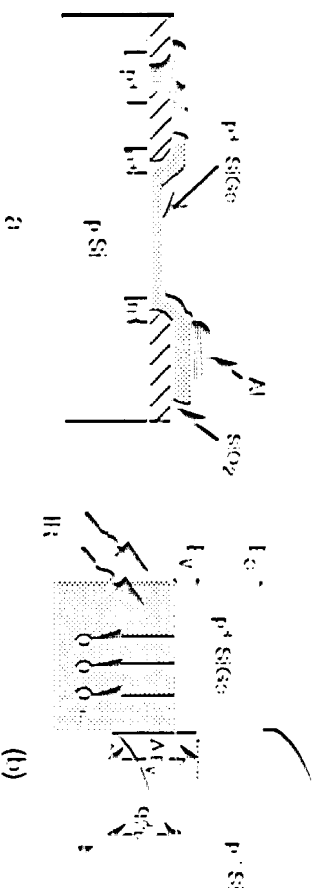


Figure 1. The schematic cross section (a) and the band diagram (b) of the Si_{1-x}Ge_x/Si HIP detector

detector idea was first demonstrated in 1990 by T. J. in et al. utilizing the advanced low-temperature molecular beam epitaxy (MBE) technology for the growth of thin, degenerately doped single-crystalline SiGe layers on Si^{3,4}. The SiGe/Si HIP detector utilized the SiGe/Si valence band offset as the potential barrier for the infrared photoemission of the photo excited holes generated in the degenerately-doped Si_{1-x}Ge_x electrode. The schematic cross section of the Si_{1-x}Ge_x/Si HIP detector and the band diagram are shown in Fig. 1 (a) and (b), respectively. The effective potential barrier is given by

$$\eta = A V_b \quad (1)$$

where $A V_b$ is the valence band offset between Si_{1-x}Ge_x and Si and η is the Fermi energy in the Si_{1-x}Ge_x layer. The Si_{1-x}Ge_x/Si valence band offset increases with the Ge composition x of the Si_{1-x}Ge_x layers.

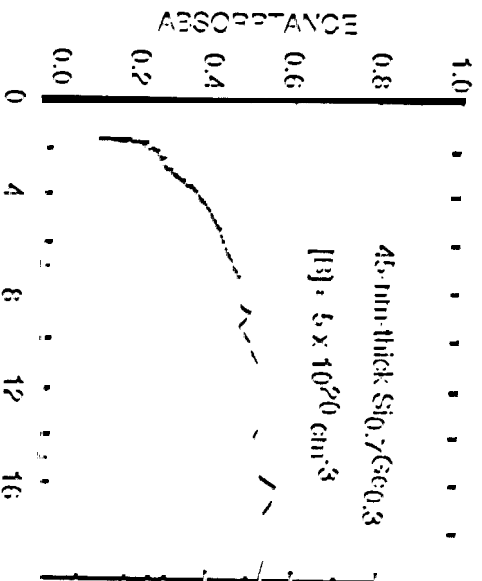


Figure 2. The absorbance measured by FTIR of a 45-nm thick $\text{Si}_{0.7}\text{Ge}_{0.3}$ layer with $[\text{B}] = 5 \times 10^{20} \text{ cm}^{-3}$.

In the degenerately doped $\text{Si}_{1-x}\text{Ge}_x$ electrode, the free-carrier absorption is the dominant mechanism for the generation of the photo excited holes⁴. The free-carrier absorbance A increases with the increasing carrier concentration and the increasing wavelength⁵, and is given by

$$A \propto N^2 \lambda^2 \quad (2)$$

where a and b are constants and N is the doping concentration. Figure 2 shown the absorption of a 45-nm-thick $\text{Si}_{0.7}\text{Ge}_{0.3}$ layer with $[\text{B}] = 5 \times 10^{20} \text{ cm}^{-3}$. Due to the degenerately doping concentration, strong absorption was observed which increases with increasing wavelength, which is beneficial for FTIR detection, and saturates in the long wavelength region. The degenerately doping concentration required for strong IR absorption results in a relatively large Fermi energy E_F . Consequently, the cutoff wavelength of the $\text{Si}_{1-x}\text{Ge}_x/\text{Si}$ MIP detector can be tailored by varying the Ge composition and the doping concentration of the $\text{Si}_{1-x}\text{Ge}_x$ layers.

2. MODEL

The detection mechanism of $\text{Si}_{1-x}\text{Ge}_x/\text{Si}$ MIP detector is similar to that of PtSi Schottky detector, involving the absorption of the incident photons in the $\text{Si}_{1-x}\text{Ge}_x$ emitter layer followed by the internal photoemission of the photo excited holes over the SiGe/Si heterojunction barrier into the Si substrate³. However, the spectral response of the $\text{Si}_{1-x}\text{Ge}_x/\text{Si}$ MIP detector differs from that of PtSi Schottky detector due to the wavelength-dependent free-carrier IR absorption and the semiconductor band structure in the degenerately doped SiGe layer. In contrast to the monotonically decreasing spectral response of the PtSi detector, which is given by the modified Fowler equation⁶

$$\eta = 1.24 C_1 \lambda \left(\frac{1}{\lambda_c} - \frac{1}{\lambda_c'} \right)^2, \quad (3)$$

where C_1 is the Fowler emission coefficient and λ is the wavelength, the spectral response of the MIP detector increases initially with increasing wavelength, and then decreases monotonically to zero at the cutoff wavelength.

Previously, a theoretical model for the internal quantum efficiency of the $\text{Si}_x\text{Ge}_{1-x}/\text{Si}$ MIP detector was reported by Tsam *et al.*⁷. The model was developed for the region $h\nu \gg E_g$, and the wavelength-dependent absorption was not considered. Because degenerate boron concentrations in the $\text{Si}_x\text{Ge}_{1-x}$ layers are usually required to obtain a strong infrared absorption, the Fermi energies are usually several hundred meV. Therefore, the previous model can only be applied in the shorter wavelength regime, i.e., for $\lambda \ll 1.24/h\nu$, and is not applicable for the determination of the cutoff wavelength and the potential barrier ψ_c . However, because a fast response increase as the wavelength decreases from the cutoff will allow the detector to have useful sensitivity near the cutoff, thereby minimizing the extension of the cutoff wavelength and associated cooling requirements, it is important to model the detector response in the spectral region near its cutoff wavelength to not only determine the potential barrier ψ_c , but also provide a figure-of-merit for evaluating the detector performance⁸.

The quantum efficiency (Q_c) η is defined as the ratio of the collected holes N_c to the incident photons N_p . Under the zero temperature approximation, and assuming $E_g = 0$, N_c is given by

$$N_c = \frac{\int_{E_g}^{E_g+h\nu} f_g(E) p(E) dE}{\int_{E_g}^{E_g+h\nu} f_g(E) p(E) dE} = \frac{1}{8} \frac{N_c (h\nu - \psi_c)^2}{\sqrt{E_g} \psi_c} \quad \text{for } h\nu > \psi_c. \quad (4)$$

$$N_c = \int_{E_j + \psi_0}^{E_j + hv} g(E) p(E) dE \approx \frac{1}{8} N \frac{(hv - \psi_0)^2}{\sqrt{E_j + \psi_0}} \quad \text{for } hv \geq \psi_0, \quad (4)$$

where $p(E)$ is the probability of emission of photo excited holes over the energy barrier⁷, and $g(E)$ is the density of states, given by $g(E) = N \sqrt{E - E_j}$, where N is an energy-independent constant. The analysis will be limited to the case $hv < E_j$ because determining the optical barrier and the spectral response near the cutoff wavelength are the primary concerns. N_p is given by

$$N_p = \frac{N_T}{A} = \frac{\int_{E_j + \psi_0}^{E_j + hv} N E^{0.5} dE}{A} = \frac{N hv E_j^{0.5}}{A} \quad \text{for } hv \ll E_j, \quad (5)$$

where A is the absorbance and N_T is the number of photo excited holes. Therefore, η is given by

$$\eta = \frac{A}{8 E_j^{0.5} (E_j + \psi_0)^{0.5}} \frac{(hv - \psi_0)^2}{hv} \quad (6)$$

The absorbance A is relatively wavelength-independent in the long wavelength region as shown in Fig. 2. Therefore, Eq. 6 reduces to the well-known Fowler equation

$$\eta = C_1 \frac{(hv - \psi_0)^2}{hv} = 1.24 C_1 \lambda \left(\frac{1}{\lambda} - \frac{1}{\lambda_c} \right)^2 \quad (7)$$

$$C_1 = \frac{A}{8 E_j^{0.5} (E_j + \psi_0)^{0.5}} \quad (8)$$

and the responsivity R is given by

$$R = C_1 \lambda^2 \left(\frac{1}{\lambda} - \frac{1}{\lambda_c} \right)^2 \quad (9)$$

The dark current characteristics of the $\text{Si}_{1-x}\text{Ge}_x/\text{Si}$ HEP detector is thermionic emission limited^{7,8}, given by

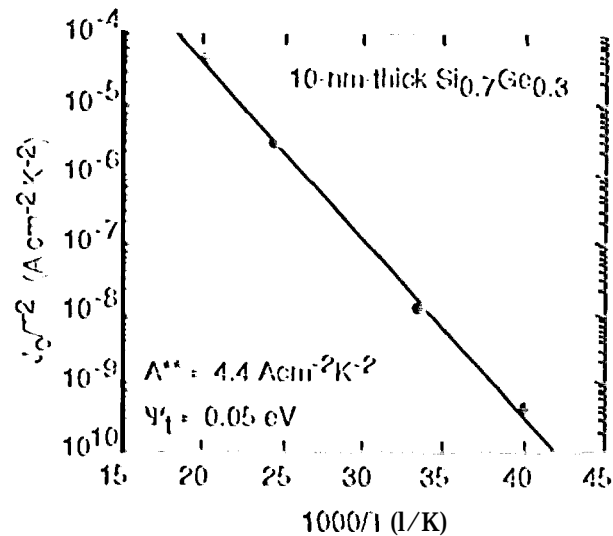


Figure 3. Plot of J_0/I^2 versus $1000/T$ for the $\text{Si}_{0.7}\text{Ge}_{0.3}/\text{Si}$ HEP detector at -0.5 V bias.

$$J_0 = A_D A^{**} T^2 \exp(-1.24/k_B T), \quad (10)$$

where A_D is the dc. vice area and A^{**} is the Richardson constant. The current noise of the $\text{Si}_{1-x}\text{Ge}_x/\text{Si}$ HEP detector is dominated by the dark current noise, given by

$$i_n = \sqrt{2 q I_0 \Delta f}, \quad (11)$$

where Δf is the noise bandwidth. Therefore, the detectivity D^* is given by

$$D^* = \frac{R}{i_n} \sqrt{A_D \Delta f} \quad (12)$$

3. DETECTOR FABRICATION

The $\text{Si}_{0.7}\text{Ge}_{0.3}/\text{Si}$ HEP detectors were fabricated by growing degenerately doped p-type hetero epitaxial $\text{Si}_{0.7}\text{Ge}_{0.3}$ layers on double-side polished p-type Si (100)

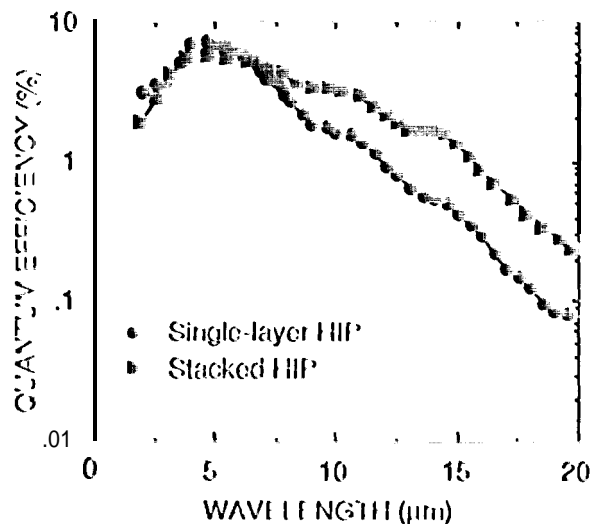


Figure 4. External quantum efficiency vs. wavelength for the single-layer $\text{Si}_{0.7}\text{Ge}_{0.3}/\text{Si}$ HIP detector (●) and stacked HIP detector (■).

in Fig. 4, the QE of $\text{Si}_{0.7}\text{Ge}_{0.3}/\text{Si}$ HIP detector initially increased with increasing wavelength to ~ 8% at 4.5 μm and then decreased. The initial increase of efficiency of the $\text{Si}_{0.7}\text{Ge}_{0.3}/\text{Si}$ HIP detector resulted from the increase of the free-carrier absorption, as shown in Fig. 1.

Figure 5 (a) shows the modified Fowler plot of $\ln(\eta/h\nu)$ versus $h\nu$ for the $\text{Si}_{0.7}\text{Ge}_{0.3}/\text{Si}$ HIP detector. As predicted by the preceding analysis, the plot was linear for $h\nu < \text{the Fermi energy}$. The optical potential barrier was determined to be 0.054 eV, corresponding to a cutoff wavelength of 23 μm. The 0.4 A/W C_1 observed was approximately twice the calculated value of 0.18 A/W from Eq. 8 because the model did not take the scattering of the photo excited carriers into consideration. Elastic scattering of carriers at the $\text{Si}_x\text{Ge}_{1-x}$ surface redirected the carriers toward the $\text{Si}_x\text{Ge}_{1-x}/\text{Si}$ interface, and thus increased the emission coefficient.

4.2 Stacked HIP detector

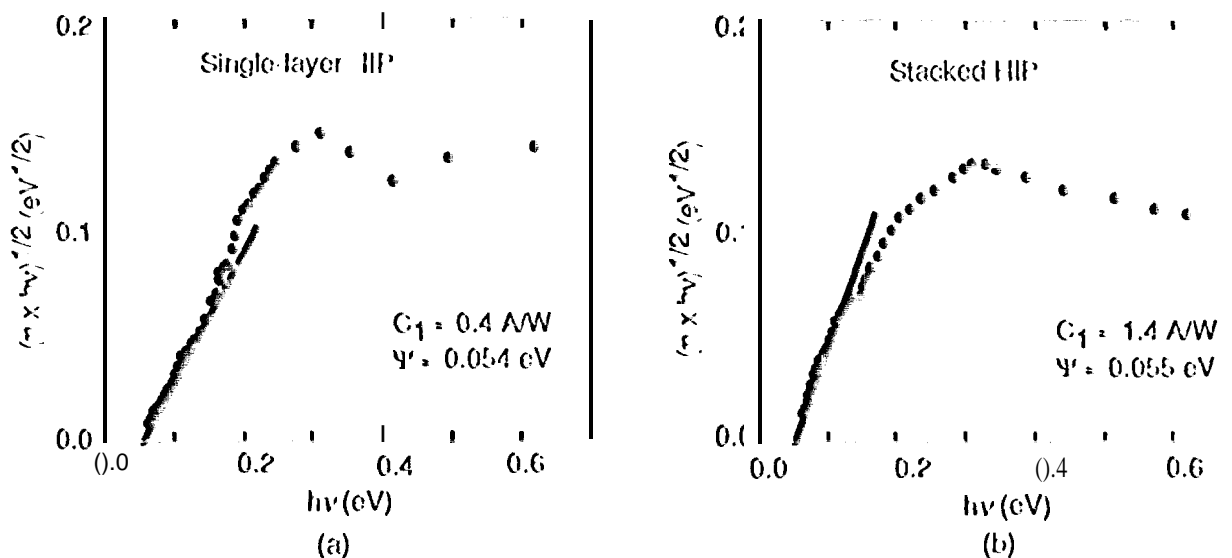


Figure 5. Modified Fowler plots of the single-layer HIP detector (a) and the stacked HIP detector (b).

wafers by MBE. The $\text{Si}_{0.7}\text{Ge}_{0.3}$ layers were grown at a substrate temperature of 350 °C using elemental boron as the dopant source. The device structure incorporates p^+ -substrate contacts and n -type guard rings which define the periphery of the active device areas to suppress edge leakage.

4. DETECTOR CHARACTERISTICS

4.1 Single-layer $\text{Si}_{1-x}\text{Ge}_x/\text{Si}$ HIP detector

Figure 3 shows the plot of J_0/I^2 versus $1/KT$ for the $\text{Si}_{0.7}\text{Ge}_{0.3}/\text{Si}$ HIP detector at -0.5 V bias. Thermionic-emission limited current characteristics were observed and the thermal potential barrier and the Richardson constant A^{**} were determined to be 0.050 eV and $4.4 \text{ Acm}^{-2}\text{K}^{-2}$. The effective barrier Ψ was significantly lower than the expected $\text{Si}_{0.7}\text{Ge}_{0.3}/\text{Si}$ valence band offset ΔE_v (~ 0.2 eV) due to the degenerate doping concentration which moved the Fermi level below the valence band edge. The external quantum efficiency for the $\text{Si}_{0.7}\text{Ge}_{0.3}/\text{Si}$ HIP detector is shown in Fig. 4. The detector was cooled to 30K and biased at -0.5 V. The spectral response was measured with front-side illumination using a 940K blackbody source. As shown

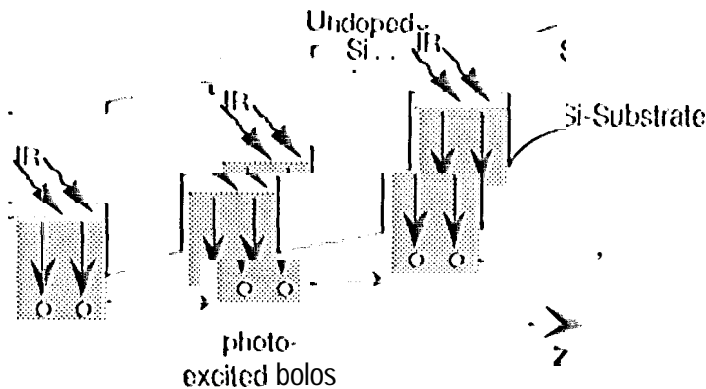


Figure 6. The band diagram of the stacked $\text{Si}_{1-x}\text{Ge}_x/\text{Si}$ HHP detector.

scattering⁹; however, reducing the $\text{Si}_{1-x}\text{Ge}_x$ layer thickness reduces infrared absorption as well. Thus, the optimal $\text{Si}_{1-x}\text{Ge}_x$ layer thickness is determined by the trade-off between absorption and internal quantum efficiency. One approach of achieving high internal quantum efficiency without losing absorption is by incorporating thin multiple absorbing $\text{Si}_{1-x}\text{Ge}_x$ layers which are stacked between Si barriers. The schematic cross-section of a stacked $\text{Si}_{1-x}\text{Ge}_x/\text{Si}$ HHP detector is illustrated in Fig. 6. The individual $\text{Si}_{1-x}\text{Ge}_x$ layer has high η_i due to the small thickness and the absorption from each layer contributes to the total absorption. Furthermore, due to the applied electric field toward the Si substrate (z-direction), the photo-excited holes traveling opposite to z-direction will be redirected toward the Si substrate. This will further increase the internal quantum efficiency.

The spectral photoresponse of a typical stacked HHP detector which consists of three 50 Å-thick p^+ - $\text{Si}_{0.7}\text{Ge}_{0.3}$ layers which are separated by 300 Å-thick undoped Si layers is shown in Fig. 4 (b). The Ge concentration and boron concentration are 30% and $4 \times 10^{20} \text{ cm}^{-3}$, respectively. The active detector areas are $1.25 \times 10^{-3} \text{ cm}^2$. The operating temperature and bias voltage are 30 K and -0.5 V (positive to the top $\text{Si}_{0.7}\text{Ge}_{0.3}$ layer), respectively. The detector shows broad photoresponse which cut off at around 20 μm . The peak response lies at around 5 μm with 6% external quantum efficiency. The response gradually decreases as the wavelength increases and a small bump is observed near 14 μm . The detector manifests about 4 and 2% external quantum efficiencies at 10 μm and 15 μm wavelengths, respectively. This stacked SiGe/Si HHP detector, in general, exhibits higher quantum efficiency in the LWIR regime ($\lambda > 10 \mu\text{m}$) than the single-layer $\text{Si}_{1-x}\text{Ge}_x/\text{Si}$ HHP detectors with the same Ge concentration, doping concentration and $\text{Si}_{1-x}\text{Ge}_x$ thickness due to the enhancement of internal quantum efficiency, especially in the long wavelength regime where photo-excited holes have small kinetic energies to cross over a potential barrier.

The modified Fowler plot of the stacked SiGe/Si HHP detector is shown in Fig. 5 (b). Similar to that of the single-layer SiGe/Si HHP detector shown in Fig. 5 (a), the plot is linear for $h\nu \ll E_b$ (~ 0.15 eV), and the potential barrier and the emission coefficient of 0.055 eV and 1.4 A/W can be determined, respectively. The higher C_j of the stacked SiGe/Si HHP detector provides a higher response near the cutoff, thereby minimizing the extension of the cutoff wavelength and the associated cooling requirements.

4.3 NEAT

The figure of merit, the noise equivalent temperature difference NEAT^{10,11}, for the $\text{Si}_{1-x}\text{Ge}_x/\text{Si}$ HHP detector can be calculated from the response model. NEAT for the $\text{Si}_{1-x}\text{Ge}_x/\text{Si}$ HHP detector in the LWIR region is given by

$$\text{NEAT} = \frac{i_n}{\int_{8 \mu\text{m}}^{\lambda_c} A R \frac{dM(\lambda)}{dT} d\lambda} \quad (13)$$

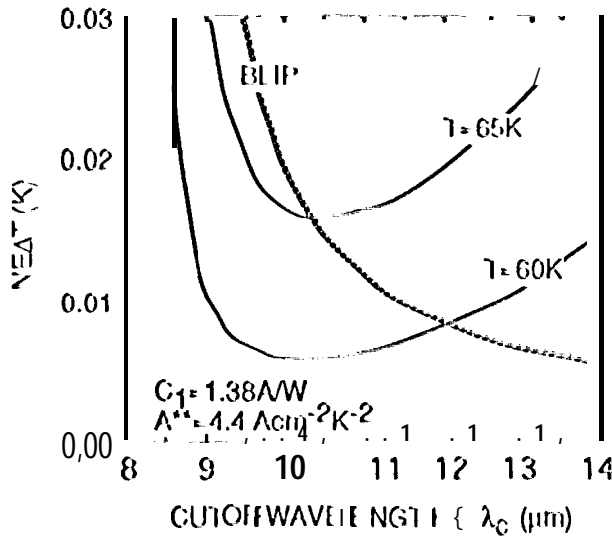


Figure 7. The calculated NEAT for the Si_{1-x}Ge_x/Si₁₁₁₁ detector at 293K background.

the thermionic emission dark current. Also shown in Fig. 7 is the background limited NEAT_B, which dominates for λ_c smaller than 10.3 μm and 12.0 μm for T = 65K and 60 K, respectively.

5. SUMMARY

Both single-layer and stacked Si_{1-x}Ge_x/Si₁₁₁₁ detectors with cutoff wavelengths of ~ 23 μm have been successfully demonstrated with thermionic emission limited dark current characteristics. A HIP photoresponse model, similar to the modified Fowler Equation was developed for wavelengths corresponding to photon energies less than the Fermi energy and agreed with the HIP detector spectral response in this wavelength region. A significantly improved C₁ was obtained for the stacked 1111 detector due to the more efficient collection of the photo-excited holes, compared to the single-layer 1111 detector.

6. ACKNOWLEDGMENTS

The work described in this report was performed by the Center for Space Microelectronics Technology, Jet Propulsion Laboratory, California Institute of Technology and was jointly sponsored by the National Aeronautics and Space Administration/Office of Advanced Concepts and Technology, the Ballistic Missile Defense Organization/Innovative Science and Technology Office, and the Air Force Rome Laboratory.

7. REFERENCES

1. W. D. Shepherd, "Infrared internal emission detectors," *SPIE Proceedings*, Vol. 1735, *Infrared Detectors: State of the Art*, edited by W. D. Shepherd, pp. 250-261, 1992.
2. W. D. Shepherd, V. E. Vickers and A. C. Yang, "Schottky-Barrier Photodiode with a High Concentration Semiconductor Active Region," U.S. Patent No. 3603847, September 7, (1971).
3. T. L. Lin and J. Maserjian, "Novel p-Si_{1-x}Ge_x/p-Si Heterojunction Infrared Detectors Fabricated by Molecular Beam Epitaxy," *Appl. Phys. Lett.*, 57, 1422, (1990).
4. T. L. Lin, T. George, E. W. Jones, A. Ksendzov and M. L. Huberman, "Elemental Boron-Doped P⁺-SiGe Layers Grown by Molecular Beam Epitaxy for Infrared Detector Applications," *Appl. Phys. Lett.*, 60, 380, (1992).
5. J. I. Pankove, *Optical Processes in Semiconductors*, (Dover Publishers, New York, 1975), p. 67.
6. V. L. Dalal, "Simple model for internal photoemission," *J. Appl. Phys.*, vol. 42, pp. 2274-2279, 1971.
7. B-Y. Tsaur, C. K. Chen and S. A. Marino, "Long-wavelength Ge_xSi_{1-x}/Si heterojunction infrared detectors and focal plane arrays," *SPIE Proceedings*, vol. 154(J), pp. S80-595, 1991.

where R and i_n are the current noise and responsivity, given by Eq. 9 and 11, respectively, and $M(\lambda)$ is the blackbody spectral radiant emittance. For the background limited NEAT_B, the current noise is dominated by the background current, and is given by

$$NEAT_B = \sqrt{\frac{2 q q \int_{8 \mu m}^{\lambda_c} A R M(\lambda) d\lambda \Delta f}{\int_{8 \mu m}^{\lambda_c} A R \frac{dM(\lambda)}{dT} d\lambda}} \quad (14)$$

Figure 7 shows the calculated NEAT for the Si_{1-x}Ge_x/Si₁₁₁₁ detector as a function of the cutoff wavelength, assuming 293K background, a 50 μm square pixel area, Δf = 60 Hz and f/2 optics at T = 60K and 65K. The initial decrease of the NEAT as the λ_c increases from the lower spectral limit of 8.1111 μm is due to the increase of the blackbody responsivity. NEAT decreases as the cutoff increases further due to the increase of

8. T. L. Lin, J. S. Park, S. D. Gunapala, E. W. Jones, and H. M. DelCastillo, "Photoresponse Model for $\text{Si}_{1-x}\text{Ge}_x/\text{Si}$ Heterojunction Internal Photoemission Long-wavelength Infrared Detector," *IEEE Electron Dev. Lett.*, Vol. 15, 103 (1994)
9. T. L. Lin, J. S. Park, S. Gunapala, E. W. Jones, and H. M. DelCastillo, "Si_{0.7}Ge_{0.3}/Si Heterojunction Internal Photoemission Long-wavelength Infrared Detector," *Optical Engineering*, **33**, 716 (1994)
10. R. H. Kingston, *Detection of Optical and Infrared Radiation* (Springer, New York, 1978).
11. F. D. Shepherd, in *Infrared Detectors and Arrays*, SPIE Vol. 930 (SPIE, Orlando, FL, 1988), p. ?.